# Spin-wave nonreciprocity and magnonic band structure in a thin permalloy film induced by dynamical coupling with an array of Ni stripes

M. Mruczkiewicz,[1] P. Graczyk,[2] P. Lupo,[3] A. Adeyeye,[3] G. Gubbiotti,[4] and M. Krawczyk[2,*]

[1]*Institute of Electrical Engineering, Slovak Academy of Sciences, Dubravska cesta 9, 841 04 Bratislava, Slovakia*

[2]*Faculty of Physics, Adam Mickiewicz University in Poznan, Umultowska 85, 61-614 Poznan, Poland*

[3]*Information Storage Materials Laboratory, Department of Electrical and Computer Engineering, National University of Singapore, 117576 Singapore*

[4]*Istituto Officina dei Materiali del CNR (CNR-IOM), Sede Secondaria di Perugia, c/o Dipartimento di Fisica e Geologia, Università di Perugia, I-06123 Perugia, Italy*

(Received 13 June 2017; published 11 September 2017)

An efficient way for control of the spin wave propagation in a magnetic medium is the use of periodic patterns known as magnonic crystals (MCs). However, the fabrication of MCs especially bicomponents, with periodicity in nanoscale, is a challenging task due to the requirement for sharp interfaces. An alternative method to circumvent this problem is to use homogeneous ferromagnetic film with a modified periodically surrounding. In this work we demonstrate that the magnonic band structure is formed in thin Py film due to dynamical magnetostatic coupling with the array of Ni stripes. We show that the band gap width can be systematically tuned by changing separation between film and stripes. We show also the effect of nonreciprocity, which is seen at the band gap edge which is shifted from the Brillouin zone boundary and also in nonreciprocal interaction of propagating spin waves in Py film with the standing waves in Ni stripes. Our findings open a possibility for further investigation and exploitation of the nonreciprocity and band structure in magnonic devices.

DOI: 10.1103/PhysRevB.96.104411

## I. INTRODUCTION

Periodic modification of materials has already been proven to be useful for tailoring propagation of electromagnetic, elastic, and spin waves (SWs). The periodicity can be introduced along one, two, or three dimensions creating band structure for waves propagating along different spatial directions. Each type of artificial crystals has many similarities common for all types of waves but also has some specific properties. Differently from electromagnetic waves which can propagate in air, SW excitations are confined to the magnetic materials and could not escape to the substrate or to the surrounding media. The formation of the magnonic bands separated by the magnonic band gaps have been demonstrated in one-dimensional (1D) and two-dimensional (2D) magnonic crystals (MCs) created by the lattice of holes, lattice of stripes or groves, and also in bicomponent structures [1–11]. A pattern introduced in thin film allows for control of the SW propagation at scales comparable to its wavelength which is suitable for integration with miniaturized devices [12,13].

The dispersion relation of long-wavelength SWs is strongly anisotropic in thin saturated ferromagnetic film, showing positive and negative slopes when waves propagate in a direction perpendicular or parallel to the magnetization, respectively. The former is a Damon-Eshbach (DE) wave [14], which is a surface wave with the amplitude concentrated at the surface of the film (this wave is also called a magnetostatic surface wave). The latter waves have bulk character and due to the negative group velocity they are called backward volume magnetostatic waves. In MCs with in-plane magnetic field the waves are additionally disturbed by inhomogeneous internal magnetic field [2,15–17]. Inhomogeneity is created by the static demagnetizing field from the edges or interfaces in the MCs. In the case of array of stripes with magnetization perpendicular to the stripe axis, the demagnetizing field strongly affects the backward waves, making conditions unfavorable for propagation [18], although propagation can be partially improved by using shallow grooves instead of stripes [19]. On the other hand, the static demagnetizing fields are absent for magnetization aligned along the stripes axis making the DE geometry preferential for investigation of the band properties. In the case of a 2D array of nanodots, the anisotropic dynamical coupling for propagating SWs has also been observed when the dispersion of collective SWs has been measured with the wave vector parallel and perpendicular to the applied field direction. This is ascribed to the anisotropic dipolar fields and the spatial distribution of the magnetic elements [20].

The surface character of SWs in the DE geometry has its origin in the magnetostatic interaction through the dynamic demagnetizing/stray field generated by the oscillating magnetization [21]. The stray magnetic field and induced electric field being outside of the ferromagnetic film can be also used to control noninvasively SW propagation [22–24]. Indeed, the metallic overlayers in the form of homogeneous film or a lattice of metallic nonmagnetic stripes have been experimentally demonstrated to modify the SW spectra and propagation properties, and in some cases, sufficient to create magnonic band structure, potentially useful for applications [25]. The SWs acquire additional property in such a structure—nonreciprocal dispersion, i.e., different SW dispersion relation for waves propagating in the opposite directions $\omega(k) \neq \omega(-k)$ [25,26]. However, there are strong limitations regarding possible miniaturization because the influence of metal with finite conductivity is related to the screening of the microwave magnetic/electric field by conducting electrons [27]. The effect is efficient when the decay of the evanescent microwave field into the metal is smaller than the metal thickness, which requires micrometer-width metallic elements [28].

*krawczyk@amu.edu.pl

 

Propagating SWs in the ferromagnetic film can be controlled also by the ferromagnetic bar deposited above a film [29,30]. The change of the magnetization orientation in the bar changes the stray magnetic field of the oscillating magnetization in the bar which couples with the SWs in the film. This mechanism was exploited to excite SWs or control the phase and amplitude of propagating SWs in a ferromagnetic stripe. The idea was further extended to the array of ferromagnetic nanodots over the ferromagnetic film. A nanodots array pumped by the microwave field at the spin wave resonance frequency has been used to induce propagating SWs in thin ferromagnetic film [31].

Very recently, analysis of thickness-modulated single (Py) and bicomponent (Py/Fe) nanowires (NWs), fabricated using developed self-aligned shadow deposition technique, have shown that layering along the third dimension is very effective for controlling the characteristics of the magnonic band. In particular, it has been found that both the frequency and the spatial profile of the most intense and dispersive mode can be efficiently tuned by the presence of the thin Fe NW overlayer. In particular, by increasing the Fe thickness, one observes a substantial frequency increase, while the spatial profile of the mode gets narrowed and moves to the permalloy NW portion not covered by Fe [32,33].

The interesting questions regarding influence of the magnetostatic interaction in bilayered structures on the magnonic bands formation arise which have not yet found an answer [34–36]. First, does the regular pattern of the ferromagnetic substrate influence the DE mode in a homogeneous thin film to create a magnonic band structure which is a characteristic feature of the MCs? If so, how sensitive is a SW dispersion relation of the layer to the presence of the stripe pattern? And finally, does the nonreciprocity of the SW dispersion in homogeneous bilayered film exist when the periodic pattern of the ferromagnetic substrate is introduced? We address these questions in our study experimentally through Brillouin light scattering (BLS) measurements of the dispersion relation of SWs in Py film deposited on the array of Ni NWs with different separation between layers and wires. The experimental data are supported and explained with the results of numerical computations. We demonstrated that in homogeneous Py film with the homogeneous internal static magnetic field the magnonic band structure is formed due to dynamic dipolar coupling with the array of the Ni NWs. We also show in micromagnetic simulations the existence of the effect of nonreciprocity in magnonic band structure due to nonreciprocal interaction between propagating SW in Py film and standing waves in Ni wires.

## II. SAMPLE STRUCTURE AND METHODS

Periodic arrays of NWs of width $w = 275$ nm, separation of $d = 215$ nm, and lattice constant $a = 490$ nm were patterned on Si substrate over a large area (4 mm × 4 mm) using deep ultraviolet lithography at 248 nm exposure wavelength. The substrate was first coated with an antireflective coating (BARC) layer of thickness of 80 nm, and a positive photoresist layer on top with a thickness of 280 nm. Details of the processing steps can be found elsewhere [37]. Cr (50 nm)/Ni (30 nm) films were then deposited subsequently on the patterned substrate using an electron beam deposition technique

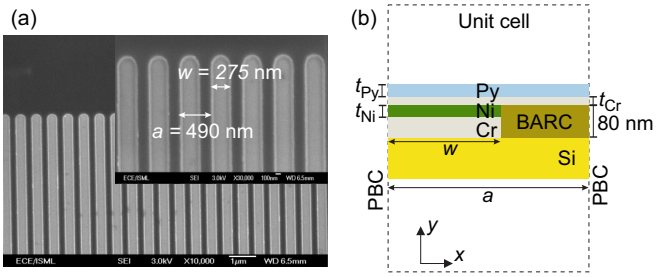


FIG. 1. (a) SEM image of the Ni wires after the first stage of the fabrication process. (b) Schematic representation of the cross-sectional view of the sample (unit cell) under investigation. It is composed of a homogeneous Py film ($t_{Py} = 30$ nm) and an array of Ni stripes ($t_{Ni} = 30$ nm) beneath it. The SWs propagate along the $x$ axis, which is perpendicular to the magnetic field (the $z$ direction). Periodic boundary conditions (PBC) are assumed along the $x$ axis.

followed by a lift-off process in OK73 thinner, resulting in arrays of Cr/Ni NWs embedded in the BARC. All the layers were deposited by electron beam evaporation in a chamber with a base pressure of $2 \times 10^{-8}$ Torr without breaking the vacuum. The thickness of the multilayer stack is identical to the BARC layer to ensure a flat film surface. Figure 1(a) shows a representative scanning electron microscopy (SEM) image of the Cr (50 nm)/Ni (30 nm) NWs array embedded in BARC matrix. In the final process, the structure obtained was covered by $Cr(t_{Cr})Ni_{80}Fe_{20}(Py,t_{Py} = 30\,nm)$ film with thickness $t_{Cr}$ varied from 0 to 30 nm. While there is possible a negligible modulation (few nanometers) at the interface between the Ni NWs and the BARC, when a thick 30 nm Py film is deposited, the Py films appears to be flat. For the control experiments, various continuous films were also deposited at the different stages of the fabrication. The scheme of cross section of the structure is shown in Fig. 1(b).

Brillouin light scattering experiments have been performed by focusing about 200 mW of monochromatic laser light with the wavelength $\lambda = 532$ nm on top of the sample using a camera objective of numerical aperture 2 and focal length 50 mm. The backscattered light was analyzed in frequency by a (3 + 3)-tandem Fabry-Pèrot interferometer. Due to the conservation of in-plane momentum, the in-plane wave vector of SW entering in the scattering process is related to the incident angle of light ($\theta$) by the following relation $k = (4\pi/\lambda)\sin(\theta)$. The SW dispersion relation was mapped across 1.5 of the Brillouin zone (BZ) by sweeping $k$ from 0 to 20 rad/$\mu$m. A magnetic field $H = 500$ Oe is applied in the sample plane along the easy direction of the Ni wires and saturates magnetization in both materials. Therefore, spectra have been recorded in the DE configuration with the magnetic field perpendicular to the incidence plane of light and to the SW wave vector ($k$) [38].

To calculate numerically SW spectra we solve the linearized Landau-Lifshitz equation (LL) in a frequency domain with damping neglected. We assume the effective magnetic field $H_{eff}$ to be a sum of three terms: $H_{eff} = H + H_{ex} + H_{dm}$. The first term is a static bias magnetic field, $H_{ex}$ is an exchange field, and the third term $H_{dm}$ is a dynamic demagnetizing field with components along the $x$ and $y$ directions. In calculations we assume that the system is extended to infinity along the $z$

axis. In that geometry the static demagnetizing field is zero. The definition of the exchange and demagnetizing fields can be found in Ref. [18]. We neglect magnetic anisotropy terms in the effective field, because its influence in materials investigated here is small. We solved LL equations in two-dimensional space for the unit cell [marked in Fig. 1(b) with a dashed line] with the periodic boundary conditions along the $x$ axis using the finite element method with COMSOL 4.3a software. From the solution of the LL equation we found frequencies of the SWs for successive wave numbers from the BZ, i.e., magnonic band structure, and spatial distribution of the SW amplitude. For more details concerning the computation method we refer to Ref. [18].

## III. EXPERIMENTAL RESULTS AND DISCUSSION

### A. Homogeneous bilayers

We start a discussion from analysis of the dispersion relation in the reference structure, which consists of two homogeneous ferromagnetic films in direct contact. The dispersion relation measured with BLS for the bilayer composed of two 30 nm thick films of Py and Ni in direct contact is shown in Fig. 2. The BLS spectra were acquired by focusing the laser beam on the top of the Py surface [see Fig. 1(b)]. The small penetration depth of light in metals, which usually does not exceed a dozen nanometers, causes the main contribution to the collected in the spectrometer signal to come from the uppermost Py continuous film. Thus a single excitation in the spectra in Fig. 2(a) can relate to the SW in Py film.

In Fig. 2(a) the BLS spectra for $k = 13.9\,\mathrm{rad}\,\mu\mathrm{m}^{-1}$ shows significantly different frequencies for peaks from the Stokes (negative frequency shift) and anti-Stokes (positive frequency shift) side of the spectra. The points for different incidence angles of light, and thus different wave numbers, are collected in Fig. 2(b). The red one shows the frequency from the anti-Stokes side (along $+k$ direction) and the black one shows the frequency from the Stokes side (along $-k$) of the BLS spectra. Both lines show the dispersion relation as expected for the magnetostatic SW of the DE type in bilayered film [39,40]. The dispersion starts around 7 GHz at $k = 0$, the frequency monotonously grows with increasing wave number but the slope depends on the sign of $k$. With increasing $k$ a difference between frequencies of waves propagating in opposite directions $\Delta\nu(k) = \nu(k) - \nu(-k)$ increases, reaching almost 3 GHz at $k = 20\,\mathrm{rad}\,\mu\mathrm{m}^{-1}$. The nonreciprocity increases almost linearly with increasing wave number as shown in Fig. 2(c). It is expected that with further increase of $k$ up to the exchange-dominated region, the $\Delta\nu(k)$ will deviate from linear behavior, reach maximum, and start to decrease [34,36]. We note that the linear dependence $\Delta\nu(k)$ in Fig. 2(b) is similar to the nonreciprocity induced by interfacial Dzyaloshinskii-Moriya interactions in the ultrathin ferromagnetic films in contact with a heavy metal. In our case the origin of the nonreciprocity is only in dynamic dipolar interactions between ferromagnetic layers and it can exist in much thicker ferromagnetic films.

The numerical results for a homogeneous bilayer film are shown in Fig. 2(b) with solid lines for waves propagating in the Py film to the right (red) and to the left (black). The dispersion relation for waves propagating in Ni film lies at lower frequencies below 6 GHz, and it is not shown here, because it is not detectable in BLS. The reasonable fit to the experimental results has been found for Ni : $M_S = 0.45 \times 10^6$ A/m and exchange constant $A = 0.8 \times 10^{-11}$ J/m, for Py : $M_S = 0.76 \times 10^6$ A/m and $A = 1.1 \times 10^{-11}$ J/m (the same parameters are used in the following part for the structures with Ni NWs). However, when the films were assumed to be in direct contact (full exchange coupling) the nonreciprocity was too small as compared to the values measured in BLS, for any choice of $M_S$. On the other hand, full separation of Py and Ni (exchange decoupled layers) results with too large nonreciprocity, whenever the frequency level at $k = 0$ is matched with the experimental result. Therefore, to obtain agreement with the BLS data we have to introduce a small separation between Py and Ni films with a layer of very small exchange coupling. A decrease of the Ni thickness of Ni by 2 nm and introduction of 2 nm thick interlayer with the exchange constant two orders smaller than in Ni: $A_{\mathrm{int}} = 0.8 \times 10^{-13}$ J/m, allowed us to obtain a reasonable match with BLS data shown in Fig. 2(b). The separation between Py and Ni with weak exchange coupling, as suggested

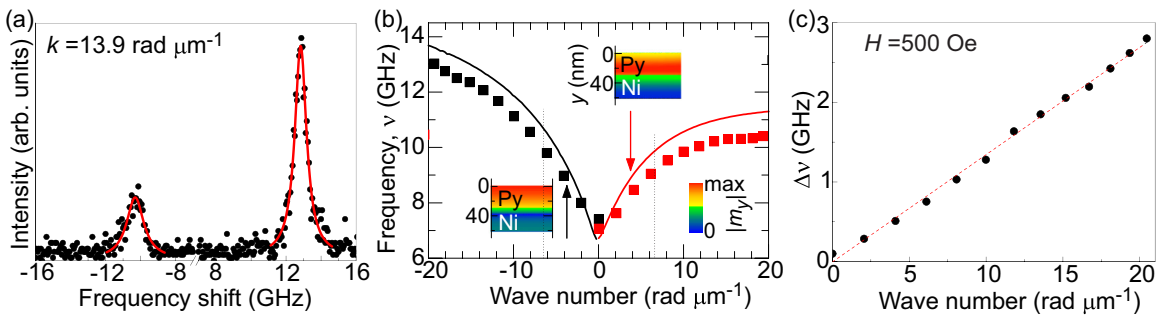


FIG. 2. Measured BLS spectrum (points) and fitted Lorentzian curve of the peaks on the Stokes and anti-Stokes side of the spectrum at $k = 13.9\,\mathrm{rad}/\mu\mathrm{m}$ in the bilayer composed of Py and Ni films. (b) Dispersion relation of SWs. The red (black) lines and square dots show the points collected from the anti-Stokes (Stokes) side of the spectra, i.e., from the waves propagating in the $+x$ and $-x$ direction, respectively. The dots are measured data, lines refer to the calculations. In the insets, the SW amplitude for two waves at the same wave number propagating in opposite directions is shown. (c) The difference in frequencies between SWs propagating in the opposite directions obtained from the Stokes and anti-Stokes sides of BLS spectra in (b) in dependence of the wave number for the external magnetic field 500 Oe. The red dotted line is a guide to the eye.

from the fitting procedure, can have an origin in the two step fabrication process with intermediate exposition into air. After deposition of the Ni, surface oxidation can take place, making a small separation between Ni and Py. Here the oxidation is not a controlled process, which can result in inhomogeneity, and still at some parts, preserve exchange coupling.

The nonreciprocity in the SW dispersion relation found in bilayers has its origin in the asymmetric structure and asymmetry of the dynamical magnetic stray field around the film related to a surface character of the wave, which reverses with the change of the propagation direction [2]. The effect exists also for dipole-exchange waves, where localization of the surface waves can differ from purely magnetostatic waves considered originally by Damon and Eshbach [14,36,41]. Indeed, in the insets of Fig. 2(b) we show the amplitude distribution for SWs propagating to the right and left direction along the $x$ axis for $k = 5.3\,\mathrm{rad}\,\mu\mathrm{m}^{-1}$. The amplitude is localized close to the top and bottom (close to Ni) side of the Py film for waves propagating in $-k$ and $+k$ direction, respectively. This shows that mainly surface wave with amplitude localized at the bottom surface (propagation $+k$) is affected by dynamical coupling with Ni film.

### B. Homogeneous film dynamically coupled to the lattice of wires

In the following part of the paper we will study the bilayers with a periodic pattern introduced in the Ni film, to test magnonic band structure for SWs propagating in homogeneous Py film induced solely due to dynamic magnetostatic coupling, and look for the nonreciprocity effects in the magnonic spectra. In Fig. 3 we show the results of the BLS measurements for three samples with different values of $t_{\mathrm{Cr}}$, varied in the range from 0 to 30 nm. The spectra are distinct from the dispersion relation of the homogeneous bilayers in Fig. 2(b). Overall dispersions for different $t_{\mathrm{Cr}}$ are qualitatively similar: the frequency of the lowest band starts at around 8.5 GHz at $k = 0$ and it grows monotonically in the first BZ, like a DE wave. Almost the same frequencies are found for peaks

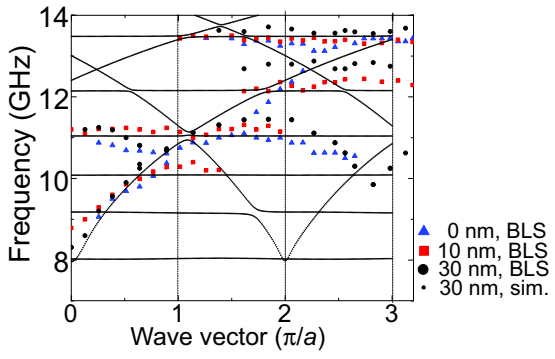


FIG. 3. The dispersion relation of SWs measured with BLS in Py film with the array of the Ni wires beneath it. The data for three samples with separation $t_{\mathrm{Cr}} = 0, 10$, and 30 nm between Py film and Ni NWs are shown. The magnetic field is in-plane of the film and along Ni wires, it has magnitude 500 Oe. The vertical dashed lines mark the Brillouin zone boundaries. The thin lines (dense small dots) mark the numerical results for Py film and Ni NWs with separation $t_{\mathrm{Cr}} = 30$nm and pinning on the Py surface.

from the Stokes and anti-Stokes side of the BLS spectra, suggesting a negligible frequency nonreciprocity. However, closer inspection of the spectra at the border of the first BZ shows that the maximum frequency of the first band does not appear exactly at the BZ boundary, but is shifted towards the higher wave numbers, $k \approx 1.07$ $[\pi/a]$. This feature is an indication of the nonreciprocity of SWs as was shown in Refs. [26,28]. For higher wave numbers (in the second BZ) a small decrease of frequency of the first band can be observed for the sample with $t_{\mathrm{Cr}} = 10$ nm. The second band in all samples has a slight negative slope near the BZ boundary, and differences between the bands from different samples can be pointed out. The last two features are a demonstration of the properties characteristic for the band structure in MCs. In the second BZ, the second band continues the trend of the dispersion of DE mode (it is clearly visible for $t_{\mathrm{Cr}} = 0$ nm). At higher frequencies, starting from 12 GHz, there are other modes which are dispersionless or have very weak dependency of frequency on $k$. The frequency of these weakly dispersive lines changes with $t_{\mathrm{Cr}}$, thus pointing at their dependence on the magnetostatic interaction between Py film and Ni stripes. The origin of these bands is not clear. The weak dependence on the wave number can suggest the dynamics in Py film induced by the standing wave excitations resonating through the width of the Ni stripes, or the higher folded back bands of the magnonic band structure.

Clearly the dispersion for Py film with Ni wires shown in Fig. 3 is distinctly different from the dispersion for homogeneous bilayer [Fig. 2(b)]. That points at an important influence of the pattern of the Ni film on the propagating SWs in the Py film. To have deeper insight into these effects, we perform calculations for Py film with Ni NWs taking the same parameters as in the bilayered structure (with 2 nm thick layer on the top of Ni wires with small $A_{\mathrm{int}}$). However, the results did not match with the BLS measurements shown in Fig. 3. The calculated dispersion was at significantly lower frequencies (it starts at 7 GHz) than in BLS spectra. The change of the magnetization saturation alone does not allow us to fit with the experimental data. We need to introduce further modification to the model.

During the fabrication process (deposition of Cr and Py layers on the already patterned sample composed of BARC and Ni) the appearance of surface roughness is unavoidable. Roughness changes the conditions for magnetization dynamics locally at the interface, which effectively can change a magnetic anisotropy on the Py surface [42,43]. Let us assume that at the bottom surface of Py film (at the interface with Cr/Ni) small surface magnetic anisotropy is induced, which results in pinning of the magnetization dynamics. To test the influence of the surface anisotropy, we performed computations with the Rado-Weertman boundary condition [44] superimposed on the dynamic part of the magnetization vector at the bottom surface of Py film [Fig. 1(b)]:

$$pm_i + \frac{\partial m_i}{\partial x} = 0,$$

with $p$ being a pinning parameter directly connected with the surface anisotropy energy [45], and $i$ indexes dynamical components of the magnetization vector ($i = x, y$) [46].

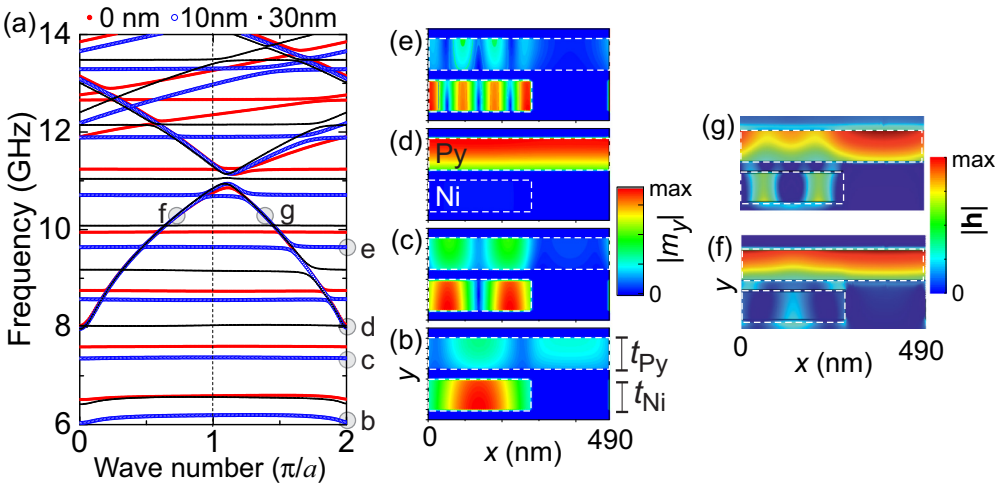


FIG. 4. (a) Magnonic band structure computed for the Py film with the array of Ni wires separated by 0, 10, and 30 nm of Cr. The vertical dashed line points at the first Brillouin zone border. The empty circles labeled (b)–(e) indicate the modes of the sample with $t_{Cr} = 10$ nm from the second BZ, which are equivalent to the BZ center. Their SW amplitude space distributions are shown in (b)–(e). (f) and (g) The magnitude of stray dynamic magnetostatic field for DE mode with the same frequency (10.3 GHz) but opposite slopes, equivalent to the waves propagating in opposite directions.

The use of $p = 0.043\,\mathrm{nm}^{-1}$ (it corresponds to the surface anisotropy energy $4.7 \times 10^{-4}\,\mathrm{J/m^2}$ at the surface of Py film [47]) allows us to match reasonably well the results of calculations with the BLS data, keeping all other parameters the same as in simulations of the bilayered structure. The results of simulations for $t_{Cr} = 30$ nm are compared with the experimental dispersion relation in Fig. 3. We fixed this value of $p$ for further investigations.

The magnonic band structure calculated for three different spacers between Py film and Ni wires are collected in Fig. 4(a). The obtained band structure is periodic in dependence of the wave number with the period equal to the reciprocal lattice vector ($G = 2\pi/a$) of the array of the Ni NWs. We can distinguish two types of bands, those with nondispersive (or with weak dispersion) and with dispersive character. The amplitude and phase distribution of the selected low frequency excitations are shown in b–f. From their analysis we can indicate that the nondispersive bands [Figs. 4(b), 4(c), and 4(e)] are standing SWs in the Ni stripes, which are quantized along the nanowire width, with some forced magnetization oscillations of low amplitude visible also in the Py film. The band (d), which has finite slope at $k = 0$, is a DE mode of the Py film [Fig. 4(d)]. The decrease of the SW amplitude in Fig. 4(d) at the surface close to Ni stripe for $k = 0$ is due to the pinning assumed at the bottom surface of the Py. The frequencies of DE band [the excitation measured in the BLS (Fig. 3)] for different $t_{Cr}$ almost overlap in the first BZ. With increasing $k$ the difference between frequencies increases, but only for bands with positive slope [the band marked with f in Fig. 4(a)], i.e., with $+k$ propagation. In the second BZ at $k = 2\pi/a$ the DE band with positive slope of 30 and 0 nm sample differs by 0.28 GHz, while at $k = 4\pi/a$ the difference is already 1.4 GHz. For wave propagating in the opposite direction (the band marked with g) the influence of $t_{Cr}$ is small. This is according with the strength of influence of the Ni NW on the SW propagating in the bilayered structure in Fig. 2. Obviously, in the limit $t_{Cr} \to \infty$ the dispersion relation will tend to DE dispersion of the thin Py film, which is close to the dispersion for $-k$.

The main feature of the band structure related to the periodicity is a magnonic band gap. In simulations for $t_{Cr} = 0$ the gap is found between 10.85 and 11.32 GHz at $k = 1.11[\pi/a]$, with shifted boundaries from the BZ boundary due to nonreciprocity. Increasing separation $t_{Cr}$ results in a decrease of the gap width, accompanied with the shift of the maximum (minimum) of the first (second) band towards the first BZ border, as is shown in Fig. 5(a).

There is also another interesting feature in the magnonic band structure shown in Fig. 4(a) related to nonreciprocity. Frequencies of the nondispersive bands depend on $t_{Cr}$, and there are four such bands in frequencies up to the first magnonic band gap. Some of them interact with the DE mode resulting in the anticrossing of the DE and horizontal bands, with a significant band gap between them. Interestingly, the anticrossing is significant only in the second BZ or alternatively for waves propagating in the $-k$ direction (due to equivalence $k' = k - G$). There is no (or very weak)

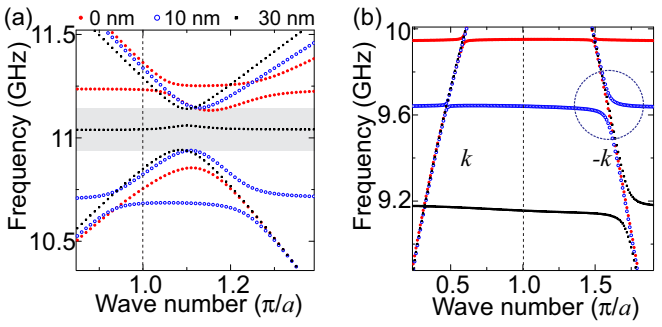


FIG. 5. Enlarged view of the dispersion relation from Fig. 4(a) around the magnonic band gap (marked with a gray bar for sample with $t_{Cr} = 30$ nm) (a), and around the anticrossings (dotted circle) of the DE band with the mode localized in Ni wires (b).

interaction for the DE wave propagating in Py along $+k$ direction, although the dispersion of $+k$ wave is most strongly affected by Ni film [see Figs. 2(b) and 4(a)]. Thus, this asymmetry in interaction between a propagating DE wave and standing waves in Ni NWs shall be related to the excitation of the standing waves in Ni NWs and asymmetric stray magnetic field generated by this confined magnetization dynamics [30]. The existence of nonreciprocal interaction between confined and propagating modes creates a good opportunity for utilization of nonreciprocity. For instance, in sample $t_{Cr} = 30$ nm at 9.18 GHz the Py film can work as a circulator or isolator for SWs at wavelength around 3 $\mu$m [see the area marked with the blue dashed line in Fig. 5(b)]. However, due to low intensity and relatively broad peaks in the BLS spectra the anticrossing has not been detected experimentally. Further investigations are required to exploit this nonreciprocal effect.

## IV. SUMMARY

We have investigated experimentally with BLS and numerically with FEM method the SW dynamics in the bilayered system composed of uniformly magnetized Py thin film and array of Ni NWs beneath Py, separated by a Cr spacer. We have shown that the dynamical magnetostatic coupling between the standing SW excitations in the wires and propagating SW in the ferromagnetic film allows us to form magnonic band structure with the band gaps for the SWs propagating in a homogeneous Py film. This proves the possibility of controlling the band properties of SWs in homogeneous film without its patterning or change of the static magnetization configuration. We found that the spacing between the wires and the film, if it is in the range of tens of nanometers, can be used to tune width of the magnonic band gap. We have also shown that in this system the nonreciprocal effects exist. The nonreciprocity is manifested in shifting of the magnonic band gap edges from the Brillouin zone border and also in the interaction between standing waves in Ni wires and propagating SWs in Py film, which depends on the direction of the propagation.

## ACKNOWLEDGMENTS

The authors thank Professor V. V. Kruglyak for fruitful discussion. The research has received partial funding from the People Programme (Marie Curie Actions) European Union's Seventh Framework Programme under REA Grant Agreement No. 609427 (Project WEST: 1244/02/01), the Slovak Academy of Sciences, the European Union Horizon 2020 Research and Innovation Programme under Marie Sklodowska-Curie Grant Agreement No. 644348 (MagIC), and National Science Center of Poland Project No. UMO-2012/07/E/ST3/00538. A.O.A. was supported by the National Research Foundation, the Prime Minister's Office, Singapore, under its Competitive Research Programme (CRP Award No. NRF-CRP10-2012-03).

[1] Z. K. Wang, V. L. Zhang, H. S. Lim, S. C. Ng, M. H. Kuok, S. Jain, and A. O. Adeyeye, Observation of frequency band gaps in a one-dimensional nanostructured magnonic crystal, Appl. Phys. Lett. **94**, 083112 (2009).

[2] S. Tacchi, G. Gubbiotti, M. Madami, and G. Carlotti, Brillouin light scattering studies of 2D magnonic crystals, J. Phys.: Condens. Matter **29**, 073001 (2017).

[3] C. L. Ordóñez-Romero, Z. Lazcano-Ortiz, A. Drozdovskii, B. Kalinikos, M. Aguilar-Huerta, J. L. Domínguez-Juárez, G. Lopez-Maldonado, N. Qureshi, O. Kolokoltsev, and G. Monsivais, Mapping of spin wave propagation in a one-dimensional magnonic crystal, J. Appl. Phys. **120**, 043901 (2016).

[4] Y. Roussigne, S. M. Cherif, C. Dugautier, and P. Moch, Experimental and theoretical study of quantized spin-wave modes in micrometer-size permalloy wires, Phys. Rev. B **63**, 134429 (2001).

[5] B. Lenk, N. Abeling, J. Panke, and M. Munzenberg, Spin-wave modes and band structure of rectangular CoFeB antidot lattices, J. Appl. Phys. **112**, 083921 (2012).

[6] R. Zivieri, S. Tacchi, F. Montoncello, L. Giovannini, F. Nizzoli, M. Madami, G. Gubbiotti, G. Carlotti, S. Neusser, G. Duerr, and D. Grundler, Bragg diffraction of spin waves from a two-dimensional antidot lattice, Phys. Rev. B **85**, 012403 (2012).

[7] S. L. Vysotskii, S. A. Nikitov, E. S. Pavlov, and Yu. A. Filimonov, The spectrum of the spin-wave excitations of the tangentially magnetized 2d hexagonal ferrite magnonic crystal, J. Commun. Techn. Electr. **55**, 800 (2010).

[8] G. Duerr, S. Tacchi, G. Gubbiotti, and D. Grundler, Field-controlled rotation of spin-wave nanochannels in bi-component magnonic crystals, J. Phys. D: Appl. Phys. **47**, 325001 (2014).

[9] S. Tacchi, B. Botters, M. Madami, J. W. Klos, M. L. Sokolovskyy, M. Krawczyk, G. Gubbiotti, G. Carlotti, A. O. Adeyeye, S. Neusser, and D. Grundler, Mode conversion from quantized to propagating spin waves in a rhombic antidot lattice supporting spin wave nanochannels, Phys. Rev. B **86**, 014417 (2012).

[10] M. Langer, F. Röder, R. A. Gallardo, T. Schneider, S. Stienen, C. Gatel, R. Hübner, L. Bischoff, K. Lenz, J. Lindner, P. Landeros, and J. Fassbender, Role of internal demagnetizing field for the dynamics of a surface-modulated magnonic crystal, Phys. Rev. B **95**, 184405 (2017).

[11] K. L. Livesey, J. Ding, N. R. Anderson, R. E. Camley, A. O. Adeyeye, M. P. Kostylev, and S. Samarin, Resonant frequencies of a binary magnetic nanowire, Phys. Rev. B **87**, 064424 (2013).

[12] S. A. Nikitov *et al.*, Magnonics: A new research area in spintronics and spin wave electronics, Phys. Uspek. **58**, 1002 (2015).

[13] M. Krawczyk and D. Grundler, Review and prospects of magnonic crystals and devices with reprogrammable band structure, J. Phys. Condens. Matter **26**, 123202 (2014).

[14] R.W. Damon and J. R. Eshbach, Magnetostatic modes of a ferromagnet slab, J. Phys. Chem. Solids **19**, 308 (1961).

[15] G. Gubbiotti, S. Tacchi, M. Madami, G. Carlotti, A. O. Adeyeye, and M. Kostylev, Brillouin light scattering studies of planar

metallic magnonic crystals, J. Phys. D. Appl. Phys. **43**, 264003 (2010).

[16] S. Choudhury, S. Saha, R. Mandal, S. Barman, Y. Otani, and A. Barman, Shape- and interface-induced control of spin dynamics of two-dimensional bicomponent magnonic crystals, ACS Appl. Mater. Interfaces **8**, 18339 (2016).

[17] B. K. Mahato, B. Rana, D. Kumar, S. Barman, S. Sugimoto, Y. Otani, and A. Barman, Tunable spin wave dynamics in two-dimensional $Ni_{80}Fe_{20}$ nanodot lattices by varying dot shape, Appl. Phys. Lett. **105**, 012406 (2014).

[18] M. Mruczkiewicz, M. Krawczyk, V. K. Sakharov, Y. V. Khivintsev, Y. A. Filimonov, and S. A. Nikitov, Standing spin waves in magnonic crystals, J. Appl. Phys. **113**, 093908 (2013).

[19] A. V. Chumak, A. A. Serga, S. Wolff, B. Hillebrands, and M. P. Kostylev, Scattering of surface and volume spin waves in a magnonic crystal, Appl. Phys. Lett. **94**, 172511 (2009).

[20] S. Tacchi, M. Madami, G. Gubbiotti, G. Carlotti, H. Tanigawa, T. Ono, and M. P. Kostylev, Anisotropic dynamical coupling for propagating collective modes in a two-dimensional magnonic crystal consisting of interacting squared nanodots, Phys Rev. B **82**, 024401 (2010).

[21] O. Gladii, M. Haidar, Y. Henry, M. Kostylev, and M. Bailleul, Frequency nonreciprocity of surface spin wave in permalloy thin films, Phys. Rev. B **93**, 054430 (2016).

[22] H. van de Vaart, Influence of metal plate on surface magneto-static modes of magnetic slab, Electron. Lett. **6**, 601 (1970).

[23] T. Yukawa, J. Yamada, K. Abe, and J. Ikenoue, Effects of metal on the dispersion relation of magnetostatic surface waves, Jpn. J. Appl. Phys. **16**, 2187 (1977).

[24] M. Mruczkiewicz and M. Krawczyk, Nonreciprocal dispersion of spin waves in ferromagnetic thin films covered with a finite-conductivity metal, J. Appl. Phys **115**, 113909 (2014).

[25] M. Inoue, A. Baryshev, H. Takagi, P. B. Lim, K. Hatafuku, J. Noda, and K. Togo, Investigating the use of magnonic crystals as extremely sensitive magnetic field sensors at room temperature, Appl. Phys. Lett. **98**, 132511 (2011).

[26] M. Mruczkiewicz, E. S. Pavlov, S. L. Vysotsky, M. Krawczyk, Y. A. Filimonov, and S. A. Nikitov, Observation of magnonic band gaps in magnonic crystals with nonreciprocal dispersion relation, Phys. Rev. B **90**, 174416 (2014).

[27] V. D. Bessonov, M. Mruczkiewicz, R. Gieniusz, U. Guzowska, A. Maziewski, A. I. Stognij, and M. Krawczyk, Magnonic band gaps in YIG-based one-dimensional magnonic crystals: An array of grooves versus an array of metallic stripes, Phys. Rev. B **91**, 104421 (2015).

[28] M. Mruczkiewicz, M. Krawczyk, G. Gubbiotti, S. Tacchi, Yu. A. Filimonov, and S. A. Nikitov, Nonreciprocity of spin waves in metallized magnonic crystal, New J. Phys. **15**, 113023 (2013)

[29] Y. Au, E. Ahmad, O. Dmytriiev, M. Dvornik, T. Davison, and V. V. Kruglyak, Resonant microwave-to-spin-wave transducer, Appl. Phys. Lett. **100**, 182404 (2012).

[30] Y. Au, M. Dvornik, O. Dmytriiev, and V. V Kruglyak, Nanoscale spin wave valve and phase shifter, Appl. Phys. Lett. **100**, 172408 (2012).

[31] H. Yu, D. Duerr, R. Huber, M. Bahr, T. Schwarze, F. Brandl, and D. Grundler, Omnidirectional spin-wave nanograting coupler, Nat. Commun. **4**, 2702 (2013).

[32] G. Gubbiotti, R. Silvani, S. Tacchi, M. Madami, G. Carlotti, Z. Yang, A. O. Adeyeye, and M. Kostylev, Tailoring the spin waves band structure of 1D magnonic crystals consisting of L-shaped iron/permalloy nanowires, J. Phys D: Appl. Phys. **50**, 105002 (2017).

[33] G. Gubbiotti, S. Tacchi, M. Madami, G. Carlotti, Z. Yang, J. Ding, A. O. Adeyeye, and M. Kostylev, Collective spin excitations in bicomponent magnonic crystals consisting of bilayer permalloy/Fe nanowires, Phys. Rev. B **93**, 184411 (2016).

[34] P. Grünberg, Magnetostatic spinwave modes of a heterogeneous ferromagnetic double layer, J. Appl. Phys. **52**, 6824 (1981).

[35] G. Gubbiotti, S. Tacchi, G. Carlotti, T. Ono, Y. Roussigné, V. S. Tiberkevich, and A. N. Slavin, Discrete modes of a ferromagnetic stripe dipolarly coupled to a ferromagnetic film: A Brillouin light scattering study, J. Phys. Condens. Matter **19**, 246221 (2007).

[36] Y. Henry, O. Gladii, and M. Bailleul, Propagating spin-wave normal modes: A dynamic matrix approach using plane-wave demagnetizating tensors, arXiv:1611.06153.

[37] A. O. Adeyeye and N. Singh, Large area patterned magnetic nanostructures, J. Phys. D: Appl. Phys. **41**, 153001 (2008).

[38] G. Carlotti and G. Gubbiotti, Magnetic properties of layered nanostructures studied by means of Brillouin light scattering and the surface magneto-optical Kerr effect, J. Phys.: Condens. Matter **14**, 8199 (2002).

[39] T. Wolfram, Magnetostatic surface waves in layered magnetic structures, J. Appl. Phys. **41**, 4748 (1970).

[40] M. S. Sodha and N. C. Srivastave, *Microwave Propagation in Ferromagnetics* (Springer Science+Business Media, New York, 1981).

[41] M. Kostylev, Non-reciprocity of dipole-exchange spin waves in thin ferromagnetic films, J. Appl. Phys. **113**, 053907 (2013).

[42] R. Arias and D. L. Mills, Theory of roughness-induced anisotropy in ferromagnetic films: The dipolar mechanism, Phys. Rev. B **59**, 11871 (1999).

[43] F. Büttner, K. Zhang, S. Seyffarth, T. Liese, H.-U. Krebs, C. A. F. Vaz, and H. Hofsäss, Thickness dependence of the magnetic properties of ripple-patterned Fe/MgO(001) films, Phys. Rev. B **84**, 064427 (2011).

[44] G. T. Rado and J. R. Weertman, Spin-wave resonance in a ferromagnetic metal, J. Phys. Chem. Solids **11**, 315 (1959).

[45] H. Puszkarski, Theory of interface magnons in magnetic multilayer films, Surf. Sci. Rep. **20**, 45 (1994).

[46] On other surfaces we have used the natural boundary conditions, on all surfaces the standard electromagnetic boundary conditions on the dynamical components of the stray magnetic field have been taken into account.

[47] N. Tahir, R. Bali, R. Gieniusz, S. Mamica, J. Gollwitzer, T. Schneider, K. Lenz, K. Potzger, J. Lindner, M. Krawczyk, J. Fassbender, and A. Maziewski, Tailoring dynamic magnetic characteristics of $Fe_{60}Al_{40}$ films through ion irradiation, Phys. Rev. B **92**, 144429 (2015).